Coupled-analysis of current transport performance and thermal behaviour of conduction-cooled Bi-2223/Ag double-pancake coil for magnetic sail spacecraft

Y. Nagasaki[a,*], T. Nakamura[b], I. Funaki[c], Y. Ashida[a], H. Yamakawa[a]

[a] *Research Institute of Sustainable Humanosphere, Kyoto University, Gokasho, Uji, Kyoto 611-0011, Japan*
[b] *Graduate School of Engineering, Kyoto University, Kyotodaigakukatsura, Nishikyo, Kyoto 615-8530, Japan*
[c] *Institute of Space and Astronautical Science, Japan Aerospace Exploration Agency, Sagamihara, Kanagawa 252-5210, Japan*

Abstract

This paper investigated the quantitative current transport performance and thermal behaviour of a high temperature superconducting (HTS) coil, and the effect of the critical current inhomogeneity along the longitudinal direction of HTS tapes on the coil performances. We fabricated a double-pancake coil using a Bi-2223/Ag tape with a length of 200 m as a scale-down model for a magnetic sail spacecraft. We measured the current transport property and temperature rises during current applications of the HTS coil in a conduction-cooled system, and analytically reproduced the results on the basis of the percolation depinning model and three-dimensional heat balance equation. The percolation depinning model can describe the electric field versus current density of HTS tapes as a function of temperature and magnetic field vector, and we also introduced the longitudinal distribution of the local critical current of the HTS tape into this model. As a result, we can estimate the critical currents of the HTS coil within 10% error for a wide range of the operational temperatures from 45 to 80 K, and temperature rises on the coil during current applications. These results showed that our analysis and conduction-cooled system were successfully realized. The analysis also suggested that the critical current inhomogeneity along the length of the HTS

*Corresponding author
Email address: nagasaki@rish.kyoto-u.ac.jp (Y. Nagasaki)

tape deteriorated the current transport performance and thermal stability of the HTS coil. The present study contributes to the characterization of HTS coils and design of a coil system for the magnetic sail spacecraft.

Keywords: HTS coil, Bi-2223, Critical current, Thermal stability, Quench current, Space application
PACS: 74.72.Hs, 84.71.Ba

---

1. Introduction

We have been studying High Temperature Superconducting (HTS) coils for a magnetic sail spacecraft. The magnetic sail is a unique spacecraft propulsion system [1]-[3], and has never been realized. The thrust of the magnetic sail is produced by the interaction between a solar wind, which is a plasma flow from the sun, and a magnetic field generated by a large-sized HTS coil. A transfer of momentum from the solar wind to the magnetic field results in a propulsive force for the sail in the direction apart from the sun. Such a so-called propellant less propulsion system has been expected to realize future deep space explorations [4]. In order to obtain an adequate driving force and high fuel efficiency and realize the magnetic sail, a magnetic moment, $\mu = NIS$, to mass ratio of the coil must be improved as large as possible. S denotes the area enclosed by the coil and NI (N: total turn number of the coil, I: operational transport current) is the magnetomotive force of the coil. One method to increase the magnetic moment is to enlarge S. Spacecraft size, however, is typically limited to be less than 4 m due to the installation size limit in the rocket for launch. Another way to increase μ is to enlarge NI. HTS coils have a big advantage for increasing I, and this is one of the major motivations to utilize the HTS coil for the magnetic sail.

Our target is to realize the magnetomotive force at 10^6-10^7 A-turns. Although YBCO coated conductors (CCs) possess high performance with respect to the critical current in high magnetic fields, Bi-2223/Ag tapes are adopted in this study. This is because the cooling characteristics of the YBCO CCs are inferior to those of the Bi-2223/Ag tapes [5] and, in addition, long length tapes with high homogeneity in the local critical currents along the length of the conductors are difficult to be available in the case of the YBCO CCs.

Reducing the weight of the spacecraft is also important for the space missions. We aim to establish a light-weight HTS coil system based on radiation

and/or conduction cooling which will utilize 3 K background temperature in space. The temperature of the installed coil, however, becomes higher than the background temperature 3 K due to the heat invasion from the sun light under such cooling condition. The coil's operating temperature must be optimized with considering the balance among the performance of the conduction-cooled HTS coil, the cooling penalty and the weight of the cooling system. Hence, estimating the performance of the conduction-cooled HTS coil for arbitrary operational temperatures is essential for the optimal coil system and operating condition for the magnetic sail.

The electric field, E, versus current density, J, characteristics of HTS tapes vary in a complicated way as a function of temperature and magnetic field vector [6]-[9]. This nonlinear $E-J$ curves are the most important factors in order to understand the coil performance, such as thermal behaviour. On the other hand, the magnetic field vector and temperature are distributed in the excited coil. This means that the $E-J$ curves are highly localized depending upon the position in the coil. In former reports, Higashikawa *et al.* made an analysis method to evaluate the current transport performance of HTS coils with taking into account the distributed $E-J$ curves, based on the percolation depinning model [10]-[13]. However, although the validity of the percolation depinning model for HTS short tapes has been precisely verified, the validity for HTS coils has not been sufficiently confirmed by experiments. In addition, the longitudinal inhomogeneity of the critical current of HTS tapes has never been considered in the analysis, although this inhomogeneity is a serious constraint factor in the case of long length tapes.

In this study, in order to realize the optimal design of the HTS coil system for the magnetic sail, we develop an analysis method to predict the current transport performance as well as thermal behaviour of a conduction-cooled HTS coil with taking into account the longitudinal distribution of critical currents of HTS tapes. We design and fabricate a conduction-cooled experimental system and a Bi-2223/Ag double-pancake coil as a scale down model system for the magnetic sail. The current transport property and thermal behaviour of the coil obtained by the analysis are compared with experimental results at various operational temperatures to validate the analysis method and the conduction-cooled system. We also investigate the effect on the coil performances of the critical current inhomogeneity in the longitudinal direction of the tape.

2. Experiment

2.1. Fabrication of scale-down model coil

In order to validate an analysis method for characterizing an HTS coil and to design the optimal coil system for the magnetic sail, we fabricated and characterized a double-pancake coil using a Bi-2223/Ag tape with a length of 200 m as a scale-down model. The tape was 4.2 mm in width and 0.28 mm in thickness, and electrically insulated with polyimide tapes.

The specifications of the fabricated coil are shown in Table 1. Total turn number was 260, and the corresponding magnetomotive force was 10^5 A-turns for 400 A, which is one order of magnitude smaller than that of our targeted coil. Fig. 1 shows the fabricated Bi-2223/Ag double-pancake coil. The coil was wound on a G10 bobbin, and the copper electrodes were soldered at both ends of the windings. Whole surface of the coil was pasted with the epoxy resin. Six pieces of aluminium sheets for cooling were symmetrically attached at both top and bottom surfaces of the coil. We firstly measured the current transport performance of the coil cooled by liquid nitrogen as a preparatory experiment.

2.2. Conduction-cooled system

Fig. 2 shows the conduction-cooled experimental system. The lowest temperature in the vacuum chamber of the cryostat can reach 4 K by the GM cryocooler and, by using a cartridge heater, the temperature can be controlled. The refrigerating capacity of the cryocooler was 1.5 W at 4 K.

2.3. Cooling structure of the coil

Fig. 3 shows (a) a schematic diagram and (b) a photograph of the inside of the vacuum chamber. The fabricated scale-down model coil was installed at the second cold-stage of the GM refrigerator. Note that the coil was on the coil supports (GFRP) and only the aluminium cooling sheets were connected to the cold-stage and cooling tower as shown in Fig. 3. From this structure, we restricted the cooling path of the coil for taking into account the cooling constraint of the spacecraft system. We also utilized the HTS current leads in order to reduce the thermal invasion from the outside of the chamber. The radiation shield walls were installed in between the voltage terminals and the coil. By introducing aforementioned cryogenic structures with trial-and-error basis, we finally developed the conduction-cooled HTS coil test system and cooled the coil down to 6 K. For the detailed examination of the

temperature distribution in the coil, we installed Cernox® thermometers at various positions of both top and bottom surfaces of the coil (see Fig. 3(b)).

3. Analysis method

3.1. Formulation of $E - J$ characteristics

Kiss *et al.* proposed the percolation depinning model for the quantitative description of the current transport properties of HTS tapes [6, 8]. Based on this model, the electric field, E, versus current density, J, properties of the HTS tapes can be expressed as a function of temperature, T, magnetic field, B, and its applied direction, ϕ [14]-[17].

$$E = \frac{\rho_{\rm FF} J_0(T, B_{\rm eq})}{m+1} \left(\frac{J - J_{\rm cm}(T, B_{\rm eq}, \sigma)}{J_0(T, B_{\rm eq})} \right)^{m+1} \quad \text{for } B_{\rm eq} \leq B_{\rm g} \tag{1}$$

$$= \frac{\rho_{\rm FF} J_0(T, B_{\rm eq})}{m+1} \left[\left(\frac{J + |J_{\rm cm}(T, B_{\rm eq}, \sigma)|}{J_0(T, B_{\rm eq})} \right)^{m+1} - \left(\frac{|J_{\rm cm}(T, B_{\rm eq}, \sigma)|}{J_0(T, B_{\rm eq})} \right)^{m+1} \right] \quad \text{for } B_{\rm eq} > B_{\rm g} \tag{2}$$

where $B_{\rm g}$ is so-called glass-liquid transition magnetic flux density. $\rho_{\rm FF}$ is the resistivity for uniform flux flow. J_0 and m are the scaling factor describing the width and the statistic parameter characterizing the shape of a critical current density, $J_{\rm c}$, distribution. $J_{\rm cm}$ is the minimum value of $J_{\rm c}$ in the distribution. In order to take into account the dependence of the applied angle of the magnetic field, we use so-called equivalent perpendicular magnetic flux density, $B_{\rm eq}$, [17] as

$$B_{\rm eq} = B(\cos^2\phi + \frac{1}{\gamma^2}\sin^2\phi)^{\frac{1}{2}} \tag{3}$$

where ϕ is an angle between the applied magnetic field and the perpendicular direction with respect to the broad surface of the tape. γ is the anisotropy ratio representing the misorientation of grains in HTS tapes as follow:

$$\gamma = \frac{B_{\rm g(\phi=90^\circ)}}{B_{\rm g(\phi=0^\circ)}} \tag{4}$$

The agreements between the percolation depinning model and experimental results of short samples ($\sim$ 30 mm length HTS tapes) were confirmed at a

variety of the amplitudes and angles of magnetic field as well as temperatures [14]-[17].

Furthermore, it was experimentally reported that the longitudinal inhomogeneity of the critical current of an HTS tape can be approximated by a Gaussian distribution [18]. We now consider this longitudinal distribution of the local critical currents by assuming that the minimum critical current density, $J_{\rm cm}$, in Eqs. (1) and (2) has a Gaussian distribution with a specific standard deviation σ in the longitudinal direction. That is, the probability density function of $J_{\rm cm}$ along the longitudinal direction in the 200 m length tape can be described as shown in Fig. 4.

3.2. Current transport performance and thermal behaviour of HTS coil

Fig. 5 shows (a) the three-dimensional (r, z, θ in cylindrical coordinates) analysis model of the double-pancake coil and (b) the flow-chart of the simulation. Since the coil is cooled only by the aluminium sheets as mentioned in section 2.3 and the amount of the radiation cooling is much smaller and can be ignored, the boundary conditions for the temperature are set as stated in Fig. 5(a). We analyse the current transport property and thermal behaviour of the HTS coil with taking into account the distributed electric field, i.e. $E_{r,z,\theta}(J, T_{r,z,\theta}, B_{r,z,\theta}, \phi_{r,z,\theta}, \sigma)$, in the coil based on the percolation depinning model. The subscript, r, z, θ, means the position of the turn in the coil. The simulation is carried out by the following steps:

STEP1: Set the initial conditions, i.e. the initial transport current, $I_{\rm op}$, operational temperature, $T_{\rm op}$, and a standard deviation, σ, of the longitudinal variation in Fig. 4.

STEP2: By using the Biot-Savart law, calculate the distribution of the self-magnetic flux density, $B_{r,z,\theta}$, and its angle, $\phi_{r,z,\theta}$, in the coil.

STEP3: The distribution of the electric field, $E_{r,z,\theta}$, in the coil is computed by substituting J, $B_{r,z,\theta}$, $\phi_{r,z,\theta}$, and the coil temperature, $T_{r,z,\theta}$, into Eqs. (1) or (2). Since the minimum critical current density, $J_{\rm cm}$, in each position in the coil is randomly determined according to the probability density function shown in Fig. 4, the calculation of the electric fields must be statistically processed [18]. The distribution of the electric filed, $E_{r,z,\theta}$, is obtained by the average value of 100 times calculations of STEP3.

STEP4: Terminal voltage, V, of the coil is computed by summing up the local electric fields, $E_{r,z,\theta}$, as Eq. (5).

$$V = \sum_{r,z,\theta} r\theta E_{r,z,\theta} \tag{5}$$

STEP5: Calculate the heat generation per unit volume by $J \cdot E_{r,z,\theta}$ and solve the three-dimensional heat balance equation by finite difference method. The temperature distribution, $T_{r,z,\theta}$, in the coil is computed.

$$C\frac{\partial T}{\partial t} = \frac{1}{r}\frac{\partial}{\partial r}\left(\kappa r\frac{\partial T}{\partial r}\right) + \frac{\partial}{\partial z}\left(\kappa\frac{\partial T}{\partial z}\right) + \frac{1}{r^2}\frac{\partial}{\partial \theta}\left(\kappa\frac{\partial T}{\partial \theta}\right) + J \cdot E \tag{6}$$

where C denotes specific heat, κ thermal conductivity, and t time. These thermal parameters of the Bi-2223/Ag tape were obtained in [5].

STEP6: STEP6 has two kinds of procedures for each section in this paper.

Section 4.1 Increase the current value of $I_{\rm op}$ and recalculate from STEP2 until the Maximum electric field in the coil exceeds 1.0 $\times 10^{-4}$ Vm^{-1}, which is the electric field criterion of the minimum critical current $I_{\rm cmin}$ [19, 20]. We finally obtain the current, I, versus voltage, V, characteristics and the critical current, $I_{\rm cmin}$, of the HTS coil.

Section 4.2 Recalculate from STEP3 at a fixed current value, $I_{\rm op}$, until the coil temperature, $T_{r,z,\theta}$, diverges or converges to a specified temperature. If $T_{r,z,\theta}$ diverges, we decrease the current value of $I_{\rm op}$, reset $T_{r,z,\theta}$ to $T_{\rm op}$, and recalculate from STEP2. We finally obtain the time evolutions of the coil temperature at fixed current values and a quench current $I_{\rm q}$. We define $I_{\rm q}$ as the maximum current value in the case that $T_{r,z,\theta}$ converges.

We quantitatively compare the analysis results with experimental ones using the scale-down model coil in order to verify the validity of this analysis method, and examine the effect on the coil performances of the longitudinal inhomogeneity of the critical current.

4. Results and discussion

4.1. Current transport performance of scale-down model coil

The current transport property of the Bi-2223/Ag scale-down model coil was firstly measured in liquid nitrogen (77 K). This cooling environment can cool the coil to 77 K uniformly, and the $I - V$ curve of the coil exactly at 77 K can be obtained. The experimental results are shown as symbols (solid circles) and the analysis results described in section 3.2 are plotted as curves in Fig. 6. In this analysis, the boundary condition of the whole coil surface for the temperature is set as the Dirichlet condition. As can be seen in Fig. 6, the analysis results agree well with the experimental ones with the standard deviation, σ, of the longitudinal inhomogeneity from 0.00 to 0.04. This result indicates that, as is well known, the longitudinal distribution of the current transport property of the Bi-2223/Ag tape is almost uniform, at least, over the length of 200 m. This is important for the practical design of the HTS coil. The agreement between the experimental result and the analysis assures the integrity of the analysis method. As can also be seen in Fig. 6, with increasing σ, the $I-V$ curve of the HTS coil is deteriorated, that is, a lower current generates a higher voltage. Our analysis results indicate that the longitudinal inhomogeneity of the critical current of the HTS tape adversely affects the current transport performance of the HTS coil. The difference between the experimental and analysis result is minimized at $\sigma = 0.02$, and the standard deviation, σ, of the longitudinal inhomogeneity is set to 0.02 in the following analyses.

Fig. 7 shows the distribution of (a) the magnetic field, $B_{r,z}$, and (b), (c) electric field, $E_{r,z}$, in the cross sectional area of the double-pancake coil. These distributions are obtained by the analysis process (STEP2 and 3) at $I_{\rm op} = 63$ A and $T_{\rm op} = 77$ K. Fig. 7(a) and (b) indicate that the magnetic and electric field are highly localized in the coil [10], and Fig. 7(c) shows that, with increasing σ, the maximum electric field in the coil is increased and also more irregularly distributed. Obviously, the HTS coil's performances must be described by considering these distributions, which can easily generate the hot spot in the HTS coil. The analysis of the thermal stability of the HTS coil, described in section 4.2, is crucially important to avoid the hot spot and the quench in the coil.

Next, we measured the current transport properties of the scale-down model coil for different operational temperatures. In this experiment, the coil was set as in Fig. 3 at the conduction-cooling condition. The purpose

of these measurements is to characterize the fabricated scale-down model coil and experimental system at various operational temperatures by means of the developed analysis code. Understanding the temperature-dependence of the performance of the HTS coil is useful to determine the optimal coil system for the magnetic sail. In the analysis, the boundary condition, $T_{\rm op}$, at both top and bottom surfaces of the coil with aluminium sheets are set to the average values obtained by the top thermo-sensors and the bottom thermo-sensors in the experiments, respectively. We repeat the simulation procedure in section 3.2 from 4 to 80 K and the experiments from 45 to 80 K for obtaining the temperature-dependence of the current transport property of the scale-down model coil (here, σ is set to 0.02).

Fig. 8 shows the temperature-dependence of (a) the $I-V$ curve and (b) the critical current of the Bi-2223/Ag scale-down model coil, obtained from the experiments (symbols) and the analysis (solid curve). In Fig. 8(b), the horizontal axis is the average of the top and bottom coil temperatures, and the vertical axis is the minimum critical current $I_{\rm cmin}$, determined by the electric filed criterion as mentioned in section 3.2 (STEP 6). In Fig. 8(b), the effects of the temperature variation of the coil surfaces on the analysis results are described as error bars. Note that the analysis results of the critical current from 4 to 80 K are obtained not from the $I-V$ curve of the short sample but that of the coil itself, in which locally distributed electric field (Fig. 7) is quantitatively taken into account. We successfully estimate the $I-V$ curves and critical currents of the HTS coil at the wide range of the coil temperatures from 45 to 80 K within the errors which are caused by the temperature variation. These results indicate that the current transport property of the conduction-cooled HTS coil, including the temperature-dependence, can be sufficiently predicted on the basis of the percolation depinning model. The agreement between the experimental and analysis results also proves the integrity of the conduction-cooling system.

4.2. Thermal behaviour of scale-down model coil

Estimating the thermal stability of the HTS coil is surely important for practical operations because the minimum critical current, $I_{\rm cmin}$, described in previous section 4.1 is not consistent with the quench current, $I_{\rm q}$ (defined in section 3.2 STEP 6), of the HTS coil. We measured the temperature traces as well as its distribution on the coil during current applications under the conduction-cooled condition as in Fig. 3. The experimental results are

compared with the thermal analysis ones in order to validate our thermal analysis of the HTS coil in section 3.2.

Fig. 9 illustrates the analysis result of the distribution of the temperature rises, ΔT, on the top surface of the coil after $I_{\rm op}$ = 63 A (=$I_{\rm cmin}$) is applied for seven minutes (t = 420 s, σ is set to 0.02). Only a half circle of the coil is described because of the symmetry of the cooling structure. As can be seen in Fig. 9, ΔT are barely distributed in a circumferential direction. We obtained the consistent result in the experiment by the three top thermosensors on the coil. This result confirms that the conduction cooling system effectively functioned and cooled the coil uniformly, although the coil was cooled only by the aluminium sheets which were placed with intervals for the limitation of the cooling path.

Fig. 10 shows the time evolution of the temperature rises, ΔT, at top sensor 1 (Fig. 3(b)) on the scale-down model coil at $I_{\rm op}$ = 63, 61, or 56 A and $T_{\rm op}$ = 77 K. The experimental results are shown as symbols and the analysis as solid curves. The temperature rises obtained by the analysis agree well with the experimental ones for the various operational currents $I_{\rm op}$. This result shows that, in addition to the current transport performance, the thermal behaviour of the conduction-cooled HTS coil can be well described by the analysis based on the percolation depinning model with taking into account the cooling constraint condition. Furthermore, although the minimum critical current, $I_{\rm cmin}$, at 77 K estimated in section 4.1 is 63 A, the coil quench occurs at $I_{\rm op}$ = 63 A in the thermal analysis, i.e. the coil temperature diverges at this current as shown in Fig. 10. This result suggests that the electric field criterion, 1.0 $\times 10^{-4}$ Vm^{-1}, is not sufficient in order to avoid the coil quench especially under the conduction-cooled condition. The coil temperature converges to a specified temperature at $I_{\rm op}$ = 56 A and the quench current, $I_{\rm q}$, at 77 K is estimated as 56 A by our thermal analysis.

We perform the same analysis at different operational temperatures, and obtain the quench currents, $I_{\rm q}$, for various operational temperatures. Fig. 11 shows the analysis result of the temperature-dependence of the maximum electric field and total heat value in the coil at the coil quench. Fig. 11 also contains the relation between the $I - V$ curve and quench current, $I_{\rm q}$, for various operational temperatures. As can be seen in Fig. 11, the smaller electric field, coil voltage, and heat generation cause the coil to be quenched at the lower coil temperature. This result comes from the fact that, because the heat capacity of the Bi-2223/Ag tape decreases with the lower temperature [5], the temperature rises in the coil increases and the thermal stability of

the coil decreases at the lower coil temperature. Note that, at less than 30 K, the electric fields which are more than one order of magnitude smaller than the common electric field criterion, 1.0 $\times 10^{-4}$ Vm^{-1}, bring about the coil quenches.

Fig. 12 indicates the analysis result of the temperature-dependence of the quench current of the scale-down model coil and the influence of the longitudinal inhomogeneity on the quench current I_{q}. The quench current decreases with increasing the standard deviation, σ, of the longitudinal inhomogeneity. This result suggests that the critical current variation along the length of the HTS tape deteriorates the thermal stability of the coil and decreases the quench current I_{q}. This is caused because the local electric field, i.e. the heat generation, becomes higher and more irregularly distributed with increasing σ as shown in Fig. 7.

As can also be seen in Fig. 12, the quench current of the scale-down model coil ($\sigma = 0.02$) is estimated as more than 400 A at the temperatures less than 20 K. The fabricated coil achieved the magnetomotive force, NI, at 10^5 A-turns at 20 K, which is one order of magnitude smaller than that of our targeted magnetic sail drive coil.

5. Conclusion

We reported an analysis method to estimate the current transport properties and thermal stabilities of HTS coils, in order to design the optimal coil system for the magnetic sail spacecraft. This method made use of $E - J$ characteristics according to the percolation depinning model. Our analysis for thermal stability can estimate the current which causes an HTS coil to be quenched by solving the three-dimensional heat balance equation. The analysis showed that this quench current of the coil was not consistent with the critical current based on the electric field criterion, 1.0 $\times 10^{-4}$ Vm^{-1}. In the analysis, longitudinal inhomogeneity of the critical current of the HTS tape was considered for more precise estimation, and it was confirmed that such inhomogeneity deteriorated the current transport performance and thermal stability of the coil. We also fabricated and established a Bi-2223/Ag scale-down model coil and a conduction-cooed experimental system. We showed that the current transport performance and thermal behaviour of the coil obtained by the analysis with taking into account the cooling condition quantitatively agreed with the experimental ones at various operational temperatures. These results proved the validity of the analysis method and

the conduction-cooling experimental system for the magnetic sail drive coil. On the basis of the developed analysis code and conduction-cooling system, to design the coil system for the magnetic sail spacecraft is our future work.

acknowledgments

The authors are grateful to TOSHIBA Corporation in Japan for their support in fabricating the Bi-2223/Ag scale-down model coil. This research is partly supported by the engineering committee of the Institute of Space and Astronautical Science of the Japan Aerospace Exploration Agency.

References

[1] R. M. Zubrin, D. G. Andrews, J. Spacecraft. Rockets. 28 (1991) 197.

[2] R. M. Winglee, J. Slough, T. Ziemba, A. Goodson, J. Geophys. Res. 105 (2000) 21 067.

[3] Y. Ashida, I. Funaki, H. Yamakawa, Y. Kajimura, H. Kojima, J. Propul. Power 59 (2012) 126.

[4] H. Yamakawa *et al.*, Acta Astronaut. 59 (2006) 777.

[5] Y. Nagasaki, T. Nakamura, I. Funaki, Y. Ashida, H. Yamakawa, Cryogenic Engineering (TEION KOGAKU) 47 (2012) 589. (in Japanese)

[6] K. Yamafuji, T. Kiss, Physica C 290 (1997) 9.

[7] A. I. Kosse, A. Y. Prokhorov, V. A. Khokhlov, G. G. Levchenko, A. V. Semenov, D. G. Kovalchuk, M. P. Chernomorets, P. N. Mikheenko, Supercond. Sci. Technol. 21 (2008) 075015.

[8] M. Inoue, T. Kiss, K. Motoyama, S. Awaji, K. Watanabe, M. Yoshizumi, Y. Yamada, T. Izumi, Y. Shiohara, Physica C 469 (2009) 1443.

[9] H. Yamasaki, I. Yamaguchi, M. Sohma, W. Kondo, H. Matsui, T. Manabe, T. Kumagai, Physica C 478 (2012) 19.

[10] K. Higashikawa, T. Nakamura, T. Hoshino, Physica C 419 (2005) 129.

[11] K. Higashikawa, T. Nakamura, H. Okamoto, IEEE Trans. Appl. Supercond. 16 (2006) 578.

Table 1: Specifications of the Bi-2223/Ag scale-down model coil for the magnetic sail spacecraft.

Items	Scale-down model coil
Shape	double-pancake coil
Turn number	130 Layer × 2 stack
Inner diameter	0.200 m
Outer diameter	0.274 m
Tape width	4.2 mm
Tape length	200 m

[12] K. Higashikawa, T. Nakamura, M. Sugano, K. Shikimachi, N. Hirano, S. Nagaya, IEEE Trans. Appl. Supercond. 18 (2008) 758.

[13] K. Higashikawa, T. Kiss, M. Inoue, S. Awaji, K. Watanabe, H. Fukushima, Y. Yamada, Y. Shinohara, Physica C 469 (2009) 1776.

[14] T. Kiss, T. Nakamura, N. Mishiro, K. Hasegawa, M. Inoue, M. Takeo, F. Irie, K. Yamafuji, Proc. MT15 2 (1998) 1052.

[15] T. Kiss, T. Okamoto, IEEE Trans. Appl. Supercond. 11 (2001) 3900.

[16] H. Okamoto, T. Kiss, S. Nishimura, K. Imamura, M. Takeo, M. Kanazawa, IEEE Trans. Appl. Supercond. 13 (2003) 3683.

[17] T. Nakamura, S. Tsuchiya, A. Fujio, T. Hoshino, I. Muta, Supercond. Sci. Technol. 15 (2002) 230.

[18] T. Nakamura, Y. Takamura, N. Amemiya, K. Nakao, T. Izumi, J. Cryo. Super. Soc. Jpn. 48 (2013) 178. (in Japanese)

[19] J. Pitel, P. Kovac, J. Lehtonen, J. Paasi, Supercond. Sci. Tecnol. 14 (2001) 173.

[20] T. Z. Dai, Z. Y. Fan, J. D. Li, Y. J. Tang, S. J. Cheng, Y. Pan, J. R. Wang, Physica C 412-414 (2004) 1239.

Figure 1: Bi-2223/Ag double-pancake coil (scale-down model for the magnetic sail).

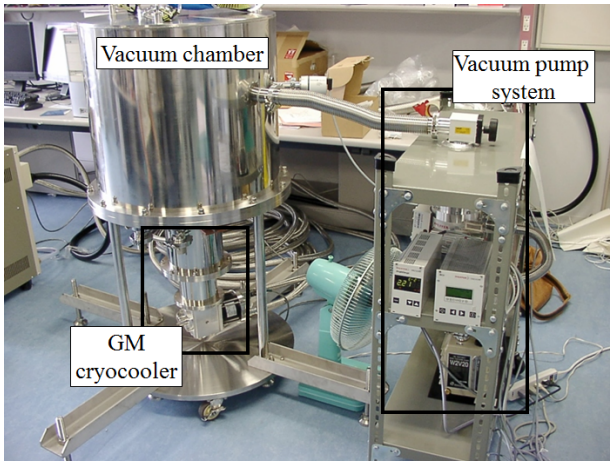

Figure 2: Conduction-cooled experimental system.

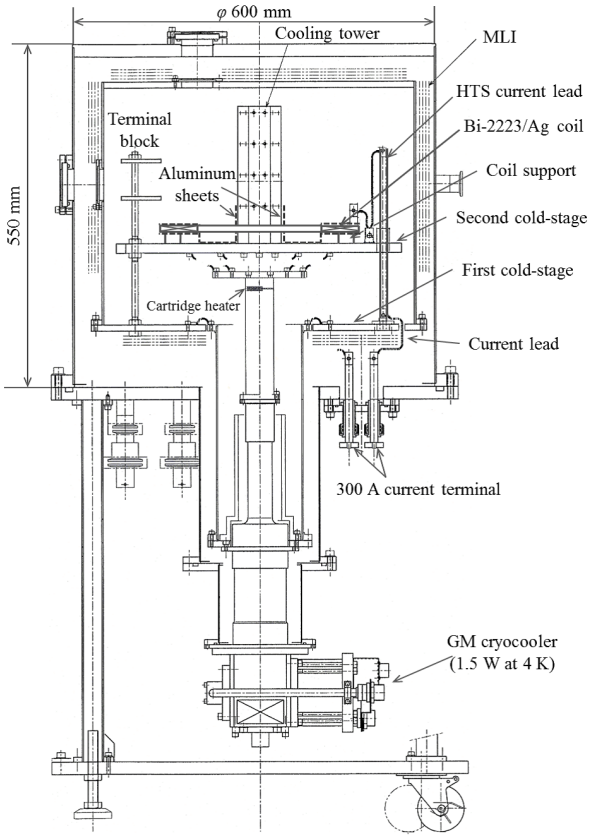

(a) Schematic diagram

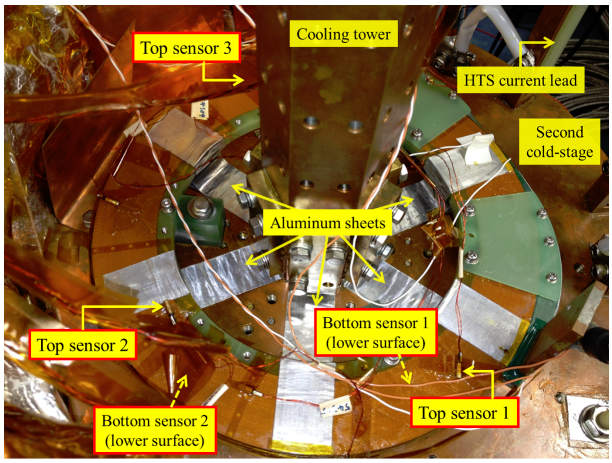

(b) Photograph

Figure 3: Cooling structure of the inside of the vacuum chamber. The second cold-stage and cooling tower were sufficiently cooled down to the operational temperature. (b) Three top thermo-sensors and two bottom thermo-sensors were installed at the surfaces of the coil.

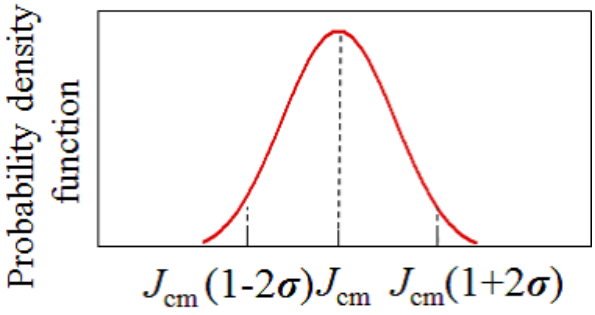

Figure 4: Probability density function of the minimum critical current, J_{cm}, along the longitudinal direction in the HTS tape.

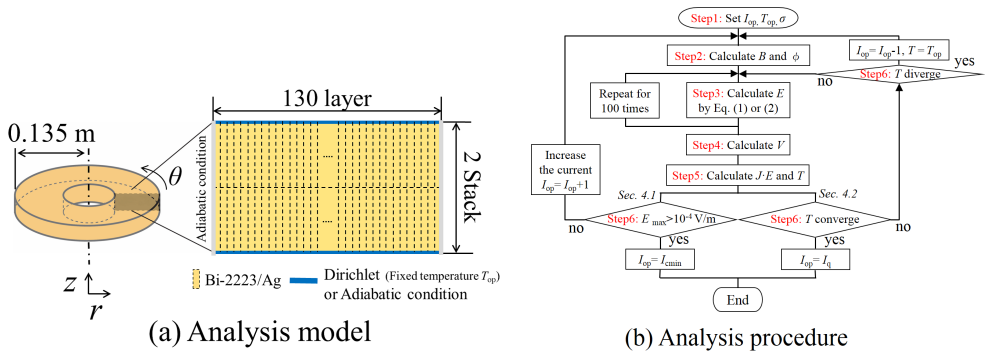

Figure 5: (a) Three-dimensional analysis model and (b) flow-chart of estimating the $I-V$ characteristics or the thermal behaviour of the HTS coil. (a) The Dirichlet condition is set at the top and bottom surfaces with the aluminium sheets, and the Adiabatic condition is set at the other surfaces.

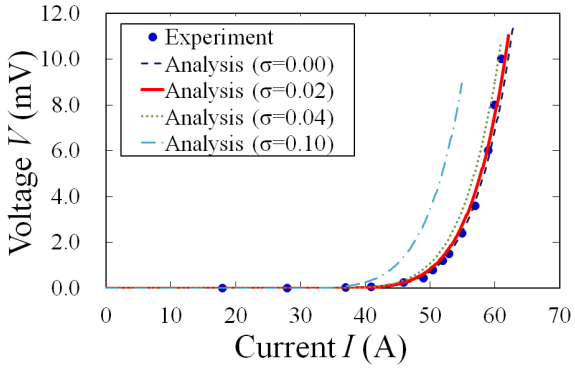

Figure 6: $I-V$ characteristic of the scale-down model coil cooled by liquid nitrogen (77 K). In the analysis, the standard deviation, σ, of the longitudinal inhomogeneity is changed from 0.00 to 0.10.

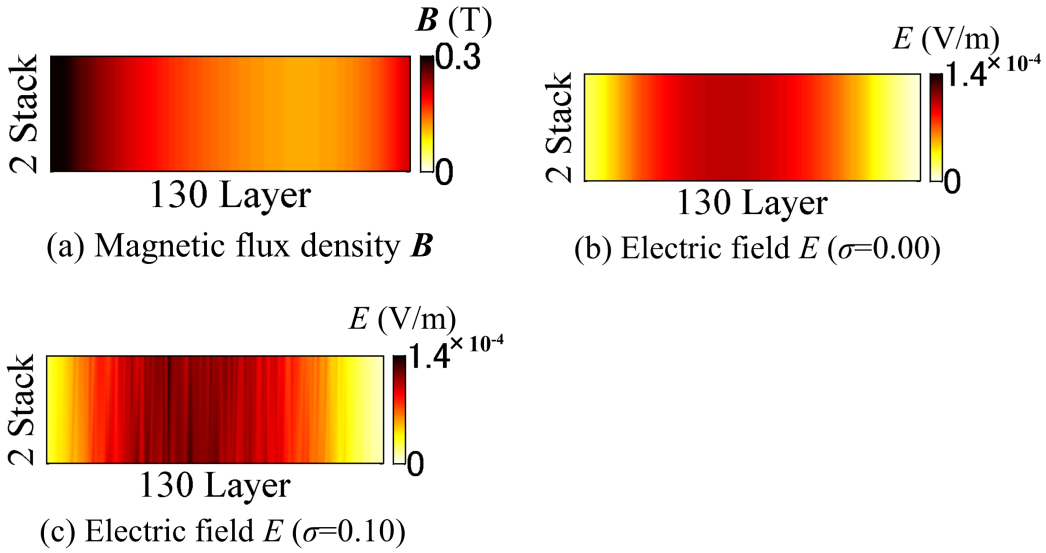

Figure 7: Analysis results of the distribution of (a) the magnetic and (b), (c) electric field in the cross sectional area of the scale-down model coil described in Fig. 5(a) ($I_{\rm op}$ = 63 A, $T_{\rm op}$ = 77 K). (b) σ = 0.00, (c) σ = 0.10.

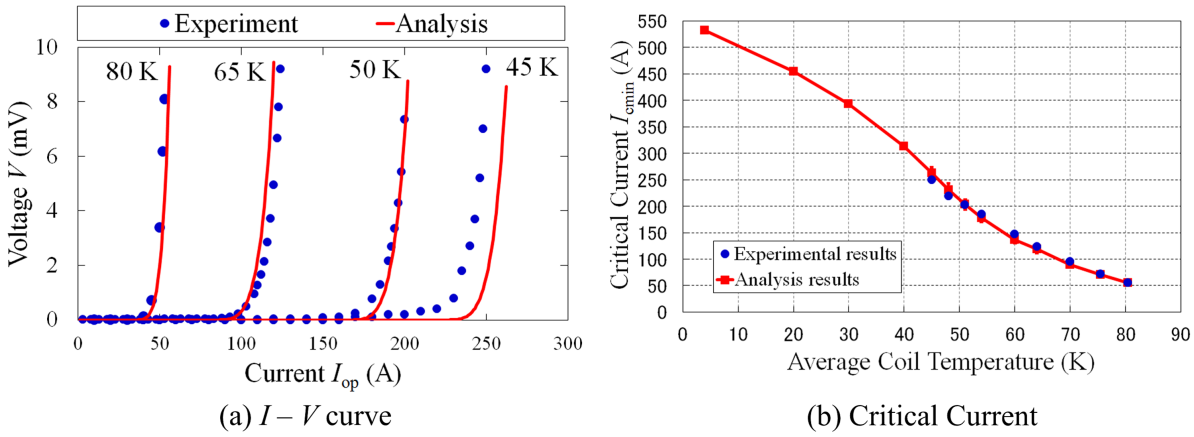

Figure 8: Temperature-dependence of (a) the $I-V$ curve and (b) the critical current of the Bi-2223/Ag scale-down model coil ($\sigma = 0.02$).

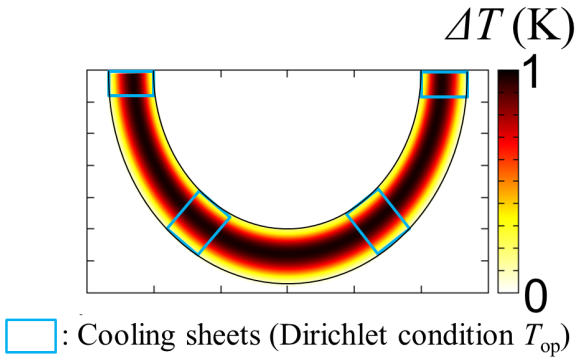

Figure 9: Analysis result of the distribution of the temperature rises, ΔT, at the top surface of the scale-down model coil ($I_{op} = 63$ A, $T_{op} = 77$ K, $t = 420$ s, $\sigma = 0.02$).

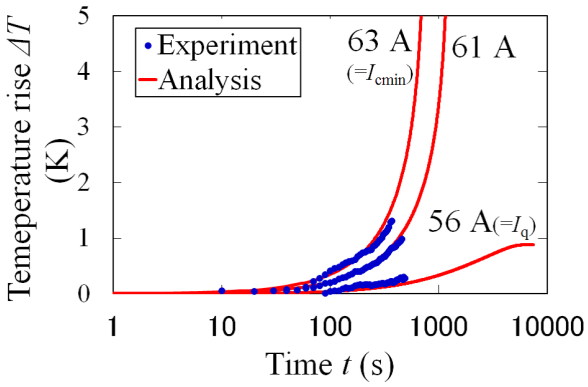

Figure 10: Time evolution of the temperature rises, ΔT, at top thermo-sensor 1 in Fig. 3(b). The currents ($I_{\rm op}$ = 63, 61, 56 A) were applied from t = 0 s (σ = 0.02, $T_{\rm op}$ = 77 K).

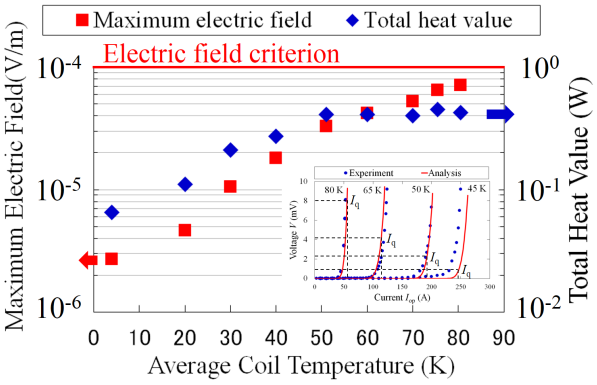

Figure 11: Analysis result of the temperature-dependence of the maximum electric field, terminal voltage, and total heat value in the scale-down model coil at the coil quench (σ = 0.02).

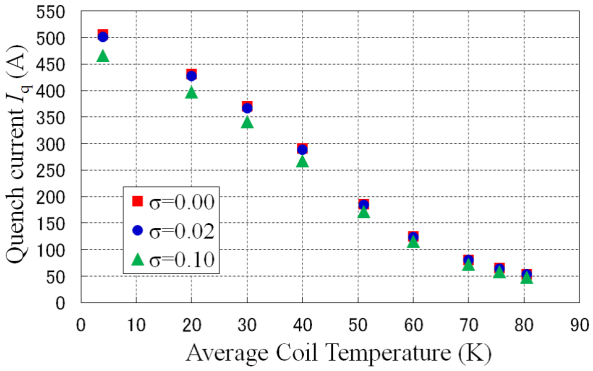

Figure 12: Analysis result of the temperature-dependence of the quench current of the Bi-2223/Ag scale-down model coil ($0.00 \leq \sigma \leq 0.10$).